AFRL-RQ-WP-JA-2012-0233

STOCHASTIC MODELING OF STRUCTURAL UNCERTAINTY/VARIABILITY FROM GROUND VIBRATION MODAL TEST DATA (POSTPRINT)

Javier Avalos and Marc P. Mignolet

Arizona State University

Eric D. Swenson

Air Force Institute of Technology

Ned J. Lindsley

Lightweight and Efficient Structures Branch
Aerospace Structures Division

JULY 2012

AIR FORCE RESEARCH LABORATORY
AEROSPACE SYSTEMS DIRECTORATE
WRIGHT-PATTERSON AIR FORCE BASE, OH 45433-7542
AIR FORCE MATERIEL COMMAND
UNITED STATES AIR FORCE

REPORT DOCUMENTATION PAGE

Form Approved
OMB No. 0704-0188

1. REPORT DATE *(DD-MM-YY)*	2. REPORT TYPE	3. DATES COVERED *(From - To)*
July 2012	Journal Article Postprint	01 March 2010 – 01 June 2012

4. TITLE AND SUBTITLE

STOCHASTIC MODELING OF STRUCTURAL UNCERTAINTY/VARIABILITY FROM GROUND VIBRATION MODAL TEST DATA (POSTPRINT)

5a. CONTRACT NUMBER
In-house

5b. GRANT NUMBER

5c. PROGRAM ELEMENT NUMBER
61102F

6. AUTHOR(S)

Javier Avalos and Marc P. Mignolet (Arizona State University)
Eric D. Swenson (Air Force Institute of Technology)
Ned J. Lindsley (AFRL/RQSE)

5d. PROJECT NUMBER
2307

5e. TASK NUMBER
N/A

5f. WORK UNIT NUMBER
A0IW0A

7. PERFORMING ORGANIZATION NAME(S) AND ADDRESS(ES)

Arizona State University
Tempe, AZ 85287-6106

Air Force Institute of Technology
Wright-Patterson Air Force Base, OH 45433
Air Force Materiel Command
United States Air Force

Lightweight and Efficient Structures Branch
(AFRL/RQSE) (formerly AFRL/VASD, and then AFRL/RBSD, Design & Analysis Methods Branch)
Aerospace Structures Division
Air Force Research Laboratory
Aerospace Systems Directorate
Wright-Patterson Air Force Base, OH 45433-7542
Air Force Materiel Command, United States Air Force

8. PERFORMING ORGANIZATION REPORT NUMBER
AFRL-RQ-WP-JA-2012-0233

9. SPONSORING/MONITORING AGENCY NAME(S) AND ADDRESS(ES)

Air Force Research Laboratory
Aerospace Systems Directorate (formerly Air Vehicles Directorate)
Wright-Patterson Air Force Base, OH 45433-7542
Air Force Materiel Command
United States Air Force

10. SPONSORING/MONITORING AGENCY ACRONYM(S)
AFRL/RQSE
(formerly AFRL/RBSD)

11. SPONSORING/MONITORING AGENCY REPORT NUMBER(S)
AFRL-RQ-WP-JA-2012-0233

12. DISTRIBUTION/AVAILABILITY STATEMENT

Approved for public release; distribution unlimited.

13. SUPPLEMENTARY NOTES

Journal article published in *Journal of Aircraft*, Vol. 49, No. 3, May–June 2012.

This in-house effort was funded via an AFOSR contract entitled, "Probabilistic Correlation between GVT and FEM for Aeroelasticity."

PA Case Number: 88ABW-2010-4684; Clearance Date: 01 Sep 2010. This technical paper contains color.

14. ABSTRACT

The focus of this investigation is on the formulation and validation of a methodology for the estimation of a stochastic linear modal model of a structure from measurements of a few of its natural frequencies and mode shapes on a few nominally identical samples of the structure. The basis for the modal model is composed of the modes of an approximate representation of the structure, e.g., a nonupdated or preliminary finite element model. Furthermore, the variability or uncertainty in the structure is assumed to originate from stiffness properties (e.g., Young's modulus, boundary conditions, attachment conditions) so that the mass matrix of the uncertain linear modal model is identity but the corresponding stiffness matrix is random. The nonparametric stochastic modeling approach is adopted here for the representation of this latter matrix; thus, the quantities to be estimated are the mean stiffness matrix and the uncertainty level. This effort is accomplished using the maximum likelihood framework using both natural frequencies and mode shapes data. The successful application of this approach to data from the Air Force.

15. SUBJECT TERMS

stochastic, variability, ground vibration test, modal analysis

16. SECURITY CLASSIFICATION OF:			17. LIMITATION OF ABSTRACT:	18. NUMBER OF PAGES	19a. NAME OF RESPONSIBLE PERSON (Monitor)
a. REPORT	b. ABSTRACT	c. THIS PAGE			Ned J. Lindsley
Unclassified	Unclassified	Unclassified	SAR	22	19b. TELEPHONE NUMBER *(Include Area Code)* N/A

JOURNAL OF AIRCRAFT
Vol. 49, No. 3, May–June 2012

Stochastic Modeling of Structural Uncertainty/Variability from Ground Vibration Modal Test Data

Javier Avalos*
Arizona State University, Tempe, Arizona 85287-6106
Eric D. Swenson†
Air Force Institute of Technology, Wright-Patterson Air Force Base, Ohio 45433
Marc P. Mignolet‡
Arizona State University, Tempe, Arizona 85287-6106
and
Ned J. Lindsley§
U.S. Air Force Research Laboratory, Wright-Patterson Air Force Base, Ohio 45433-7531

DOI: 10.2514/1.C031546

The focus of this investigation is on the formulation and validation of a methodology for the estimation of a stochastic linear modal model of a structure from measurements of a few of its natural frequencies and mode shapes on a few nominally identical samples of the structure. The basis for the modal model is composed of the modes of an approximate representation of the structure, e.g., a nonupdated or preliminary finite element model. Furthermore, the variability or uncertainty in the structure is assumed to originate from stiffness properties (e.g., Young's modulus, boundary conditions, attachment conditions) so that the mass matrix of the uncertain linear modal model is identity but the corresponding stiffness matrix is random. The nonparametric stochastic modeling approach is adopted here for the representation of this latter matrix; thus, the quantities to be estimated are the mean stiffness matrix and the uncertainty level. This effort is accomplished using the maximum likelihood framework using both natural frequencies and mode shapes data. The successful application of this approach to data from the Air Force Institute of Technology joined wing is demonstrated.

Nomenclature

E_N	=	overall fit of modal model
$\overline{K}$	=	modal model mean stiffness matrix
K_{XX}	=	covariance matrix of realized values
L	=	likelihood function
$\boldsymbol{s}_i$	=	coordinates of measurement point i
$\boldsymbol{s}_L$	=	coordinates of laser collimator
$\boldsymbol{x}^{(r)}$	=	realized values in rth experiment
$\alpha_{mj}^{(r)}$	=	measured values of modal coefficients
δ	=	uncertainty parameter
λ	=	free parameter of statistical distribution of random matrices
$\boldsymbol{\mu}_X$	=	mean vector of realized values
$\boldsymbol{\phi}_j$	=	finite element modes
$\boldsymbol{\psi}_m^{(r)}$	=	mode shapes projected basis

I. Introduction

THE U.S. Air Force is responding to new global threats by conceiving aircraft with diverse and revolutionary capabilities. These capabilities have led to trends in smaller fleet sizes, as well as more diverse flight regimes and expanded performance limits. Such a confluence of trends renders the design, analysis, and certification (DAC) of a prototype even more vital to ensuring an efficient long-lasting fleet. An integral part to the DAC process is the updating of a baseline finite element model (FEM) with ground vibration modal test results to obtain the truth model for a prototype structure. This process has traditionally been a deterministic one, yet there are indications (e.g., [1]) of a definite variability in the structural properties of one aircraft component vs another.

An important use of the updated FEM has been the construction of a reduced, modal model, which is then used in aeroelastic analyses for the prediction of the flutter speed, altitude, and frequency. The variability observed in the test data is then reflected through a similar variability of the expected flutter characteristics. It also implies an uncertainty on where/when this phenomenon might occur when using components that have not been tested.

To address this uncertainty issue, it is suggested here to first proceed with a structural modeling that directly accounts for its variability, e.g., using a probabilistic framework as will be done here. Propagating next the uncertainty through the aeroelastic computations, typically by Monte Carlo methods, will then provide the desired metrics (e.g., standard deviations, 98th percentiles) of the flutter boundary variability. In this regard, note that the consideration of the structural uncertainty can be carried out at either full FEM or modal model levels. The latter is adopted here, and a general framework for the construction of a stochastic modal model is described and validated using experimental results on the Air Force Institute of Technology (AFIT) joined wing [2].

II. Stochastic Modal Model Identification

The construction of a stochastic modal model of a structure requires three key aspects: 1) the selection of a basis, including its size and the functions that compose it; 2) the adoption of a representation of the random elements (typically the elements of the modal mass and/or stiffness matrices) of the modal model; and 3) the estimation of the deterministic parameters of this representation from experimental data.

Presented as Paper 2011-1940 at the SDM Conference, Denver, CO, 4–7 April 2011; received 14 June 2011; revision received 25 October 2011; accepted for publication 26 October 2011.

*Postdoctoral Research Associate, SEMTE, Faculties of Mechanical and Aerospace Engineering. Member AIAA.
†Assistant Professor, Department of Aeronautics and Astronautics.
‡Professor, SEMTE, Faculties of Mechanical and Aerospace Engineering. Associate Fellow AIAA.
§Senior Aerospace Engineer, AFRL/VASD.

Considering first the basis selection, two notable alternatives are possible. The first mimics the corresponding deterministic analyses in which the basis functions are intimately linked to the structural model (i.e., they are its mode shapes) and the resulting modal mass and stiffness matrices are diagonal. The direct extension of these concepts to the case of a stochastic structure leads to random basis functions with a modal stiffness (and possibly mass) matrix that remains diagonal with random elements. This representation is certainly acceptable but is generally very challenging to establish because of the need to characterize the joint distribution of the elements of the random mode shapes guaranteeing the orthogonality and normalization conditions.

A simpler approach is to rely on a fixed, deterministic basis to which will then be associated generally full stiffness and/or mass matrices. This strategy is often employed with the basis functions being the mode shapes of the mean model, but in its absence here, it is proposed to adopt the mode shapes of the baseline FEM, as they span the correct spatial domain and satisfy the proper boundary conditions. The number of such modes to include in the basis will be estimated from the experiments, as discussed next.

With the basis fixed, the randomness of the structure is localized to the elements of the corresponding stiffness (and/or mass) matrix, the statistical distribution of which must then be characterized. This task is performed here using the nonparametric stochastic modeling approach (e.g., [3,4]) in which the joint probability density function of the random (stiffness and/or mass) matrix elements is derived to achieve the maximum of the statistical entropy under specified, physical constraints. The nonparametric approach thus replaces the many distribution-related assumptions usually involved in the characterization of random structural models by a single hypothesis: the maximization of the entropy. This condition implies that the distribution of the uncertain properties will have a heavy tail, i.e., will spread as widely as is consistent with the imposed constraints. Then, a good sampling of the space of the acceptable values of these properties will be achieved.

The constraints imposed on the maximization of the entropy stem from physical requirements expected of all stiffness and mass matrices: symmetry, positive definiteness, and finiteness of the inverse (assuming that there are no rigid-body modes). It is further imposed that the mean matrix be equal to its counterpart for the mean model. With these constraints, it was shown [3] that the maximum of the entropy is maximized when the random matrices B to be simulated can be expressed as

$$B = \overline{L} H H^T \overline{L}^T \tag{1}$$

where $\overline{L}$ is any decomposition (e.g., a Cholesky decomposition) of the mean matrix $\overline{B}$, i.e., satisfying $\overline{B} = \overline{L}\overline{L}^T$. Furthermore, H denotes a lower triangular random matrix, the elements of which are all statistically independent of each other. Moreover, 1) the diagonal elements H_{ii} are obtained as $H_{ii} = \sqrt{Y_{ii}/\mu}$, where Y_{ii} is Gamma distributed with parameter $(p(i) - 1)/2$ and 2) the offdiagonal elements H_{il}, $i \neq l$, are normally distributed (Gaussian) random variables with standard deviation $\sigma = 1/\sqrt{2\mu}$, as pictorially described in Fig. 1. Note further that

$$p(i) = n - i + 2\lambda - 1 \tag{2}$$

and

$$\mu = \frac{n + 2\lambda - 1}{2} \tag{3}$$

with n denoting the size of the matrices B.

In the preceding equations, the parameter $\lambda > 0$ is the free parameter of the statistical distribution of the random matrices H and B and can be evaluated to meet any given information about their variability; often, the standard deviation of the lowest natural frequency of the random linear system will be specified and used to obtain λ. This condition, coupled with Eqs. (1–3) and properties 1 and 2, provides a complete scheme for the generation of random symmetric positive definite matrices B.

The optimization-based formulation of the nonparametric approach permits the consideration of different or additional constraints as required by the problem at hand. This observation has led to an extension [4] of the preceding, original methodology [3] in which the standard deviations of several natural frequencies are imposed. The resulting probabilistic model then exhibits more than the single parameter λ for an improved matching of available data. Furthermore, a computationally efficient simulation strategy of the corresponding random matrices B, paralleling but different from the one of Eqs. (1–3) and Fig. 1, has also been devised [4].

The preceding discussion has addressed the first two key issues in the formulation of a stochastic modal model of the structures considered. In fact, this model is completely characterized by the known basis functions and the yet unknown mean stiffness matrix $\bar{K}$ (assuming that the uncertainty is in stiffness, and thus $B = K$) and the parameter λ of the original nonparametric approach (or the parameters λ_i of the extended formulation [4]). Note that the neglect of any variability in the mass properties leads to an identity modal mass matrix if the finite element (FE) mode shapes have been normalized in this manner.

The last issue to be addressed is thus the estimation of the matrix $\bar{K}$ and parameter λ from the experimental data. In this context, it is assumed here that M natural frequencies $\omega_m^{(r)}$ and mode shapes $\boldsymbol{\psi}_m^{(r)}$ of a series of R similar structures have been measured: $m = 1, 2, \ldots, M$ and $r = 1, 2, \ldots, R$. Then, before proceeding with the estimation of $\bar{K}$ and λ, it is first necessary to reduce the available data to the modal model framework; that is, the mode shapes $\boldsymbol{\psi}_m^{(r)}$ must be projected on the basis of N ($N \geq M$) modes $\boldsymbol{\phi}_j$ of the baseline FEM. This is achieved by searching for the best representation of $\boldsymbol{\psi}_m^{(r)}$ in the form

$$\boldsymbol{\psi}_m^{(r)} \approx \sum_{j=1}^{N} \alpha_{mj}^{(r)} \boldsymbol{\phi}_j \tag{4}$$

In fact, the coefficients $\alpha_{mj}^{(r)}$ represent the mode shape m of experiment r viewed in the modal space spanned by the FE modes $\boldsymbol{\phi}_j$.

If all degrees of freedom (DOFs) of the FEM have been observed in the experiment, the determination of the modal coefficients $\alpha_{mj}^{(r)}$ can be accomplished by premultiplying Eq. (4) by the FE mass matrix and using the orthogonality properties of the modes $\boldsymbol{\phi}_j$. If not all DOFs have been observed, as is expected in connection with most large structures, the estimation of the coefficients $\alpha_{mj}^{(r)}$ can be done by a least-squares solution of the linear system of equations [Eq. (4)]. This approach will be referred to here as the original projection approach.

The overall fit of the approximation of Eq. (4) can be measured by the error

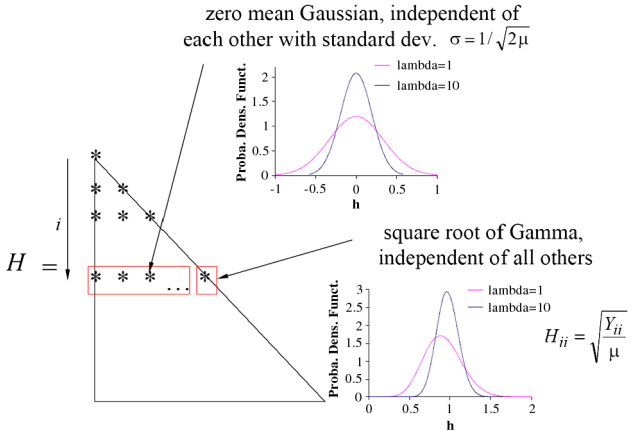

Fig. 1 Structure of the random H matrices with $n = 8$, $i = 2$, and $\lambda = 1$ and 10 (dev. denotes deviation).

$$E_N = \frac{1}{MR}\sum_{m,r}\frac{\|\boldsymbol{\psi}_m^{(r)} - \sum_{j=1}^{N}\alpha_{mj}^{(r)}\boldsymbol{\phi}_j\|}{\|\boldsymbol{\psi}_m^{(r)}\|} \tag{5}$$

where the subscript N emphasizes the dependence of the error on N, the number of FE modes. It is proposed here to select this parameter to be the lowest value for which E_N is below a specified threshold value related to the noise level in the experiments.

The estimation of $\overline{K}$ and λ may then proceed from the measurements $\omega_m^{(r)}$ and $\alpha_{mj}^{(r)}$, and a maximum likelihood approach is suggested here [5], as demonstrated in [6–9] for related problems. That is, $\overline{K}$ and λ will be determined to yield the maximum of the likelihood function

$$L = \prod_{r=1}^{R} p_X(\boldsymbol{x}^{(r)}; \overline{K}, \lambda) \tag{6}$$

where $p_X(\boldsymbol{x}; \overline{K}, \lambda)$ denotes the probability density function of the random vector

$$\boldsymbol{X} = (\Omega_1\ A_{11} \ldots A_{1(N-1)}\ \Omega_2\ A_{21} \ldots A_{2(N-1)} \ldots\ )$$

Included in this vector are the M random natural frequencies Ω_m, $m = 1, \ldots, M$, of measured values $\omega_m^{(r)}$; and the random mode shapes coefficients A_{mj}, $m = 1, \ldots, M$ and $j = 1, \ldots, N-1$, of measured values $\alpha_{mj}^{(r)}$. These random variables are derived from the stochastic modal model with random stiffnesses $\underline{K}$ defined by Eqs. (1) and (3) for the specified $\overline{K}$ and λ. Note that only the first $N-1$ component of the mode shapes are included in $\boldsymbol{X}$, as the Nth one can be extracted from the normalization condition

$$\underline{A}_m^T\,\underline{A}_m = \sum_{j=1}^{N} A_{mj}^2 = 1 \tag{7}$$

given that the modal mass matrix is identity. Furthermore, the vector $\boldsymbol{x}^{(r)}$ denotes the realized values of $\boldsymbol{X}$ in the rth experiment. That is,

$$\boldsymbol{x}^{(r)} = (\omega_1^{(r)}\ \alpha_{11}^{(r)} \ldots \alpha_{1(N-1)}^{(r)}\ \omega_2^{(r)}\ \alpha_{21}^{(r)} \ldots \alpha_{2(N-1)}^{(r)} \ldots\ ) \tag{8}$$

The estimation of $p_X(\boldsymbol{x}; \overline{K}, \lambda)$ would proceed as follows. For a given mean stiffness matrix $\overline{K}$ and uncertainty parameter λ, a large number of realizations of the random modal stiffness matrix K would be generated according to Eqs. (1–3). Then, for each one of them, the natural frequencies and mode shapes of the corresponding dynamical system would be obtained. Then, a statistical analysis of this population of frequencies and mode shapes would lead to the estimation of $p_X(\boldsymbol{x}; \overline{K}, \lambda)$. Given the expected high dimensionality of $\boldsymbol{X}$, with $p = N \times M$ components, the determination of this exact probability density function may represent a daunting task requiring an excessively large number of simulations to be carried out. An alternate approach is to approximate $p_X(\boldsymbol{x}; \overline{K}, \lambda)$ by its Gaussian counterpart (asymptotically correct as the uncertainty level goes to zero; see [10]):

$$p_X^G(\boldsymbol{x}; \overline{K}, \lambda) = \frac{1}{(2\pi)^{p/2}\sqrt{\det(K_{XX})}} \times \exp\left[-\frac{1}{2}(\boldsymbol{x} - \boldsymbol{\mu}_X)^T K_{XX}^{-1}(\boldsymbol{x} - \boldsymbol{\mu}_X)\right] \tag{9}$$

where $\boldsymbol{\mu}_X(\overline{K}, \lambda)$ and $K_{XX}(\overline{K}, \lambda)K_{XX}(\overline{K}, \lambda)$ denote the mean vector and covariance matrix of the random vector $\boldsymbol{X}$ determined from the simulations described previously for the given mean stiffness matrix $\overline{K}$ and uncertainty parameter λ. The Gaussian assumption of Eq. (9) leads to a computationally very efficient approach but may not always provide the desired close fit of the probability density function. In such situations, the more refined kernel density estimation method [11–13] could be used instead of Eq. (9) to build the likelihood function.

III. Test Article: Air Force Institute of Technology Two Meter Joined Wing

The development of persistent intelligence, surveillance, and reconnaissance (ISR) platforms is a key area of emphasis for the foreseeable future. Current airborne ISR assets can only provide limited persistent coverage, and their current sensors can only collect data over a limited area when compared with radar. The Boeing concept includes a joined-wing design, as shown in Fig. 2 [14]. The joined-wing design concept allows an aircraft to have a large wingspan due to the inclusion of an aftwing, which provides the additional required stiffness. The long wingspan provides the ability to house a large radar in order to generate long wavelengths necessary to penetrate foliage. These radar arrays will have to be fully integrated into the remotely piloted vehicle wing structure in order to keep size and weight minimal. This concept of combining the radar array and structure is referred to as the conformal load-bearing antenna structure.

To achieve high lift and low drag, the wings will have a very high aspect ratio. This concept vehicle's long endurance requirement dictates a high fuel load, a low structural weight fraction, and a high aspect ratio, and it will likely result in wings that are flexible, resulting in large deflections under load. The aftwing is present to improve structural efficiency in achieving larger wingspans without significantly increasing the structural weight required to withstand high-lift loads. It is expected that this large wingspan will have a high geometric nonlinearity with respect to external loads [15,16].

Wolkovich presented the joined-wing concept in 1986 [17]. In his paper, Wolkovich demonstrates two important advantages of the joined-wing concept: light weight and high stiffness. Early studies showed that bending due to a vertical tip load occurs in the direction perpendicular to the plane created by the axes of the fore- and aftwings [18]. Figure 3 depicts the plane created by the axes of the fore- and aftwings. For long, flexible joined wings under a large load, the applied tip load will cause bend–twist coupling in the aftwing. However, Patil noted that the joined-wing design is much stiffer than single-wing configurations, and in his tests, he also found that the joined wing can be made stiff enough to only show negligible nonlinear effects [19].

Since the joined wing's inception, there has been a wide variety of research efforts on the joined-wing concept. Snyder et al. analyzed a twin-boom fuselage sensor-craft configuration that included aeroelastic analysis using FE modeling and computational fluid dynamics [20]. Blair et al. investigated aspects of the joined-wing structure while accounting for critical loads throughout the mission envelope [21]. Smallwood investigated the joined wing and predicted a worst-case gust load response resulting in about an 8–9 deg pointing error [22]. Roberts computed predictions to a gust load response while accounting for geometric nonlinearities [23]. Bond and Canfield successfully created an all-aluminum 2 m semispan test article on which they applied static follower forces and collected nonlinear deformations [24]. They were also successful in reaching agreement between their measured displacements and strains and Nastran nonlinear analytical results. Based on lessons learned from Bond and Canfield's work, a 2 m joined-wing test article was designed and built at AFIT, which is discussed next.

The primary test article discussed in this research effort is a 2 m joined wing, as shown in Fig. 4, which has a winglike cross section. The fore- and aftwings are solid aluminum with cross-section

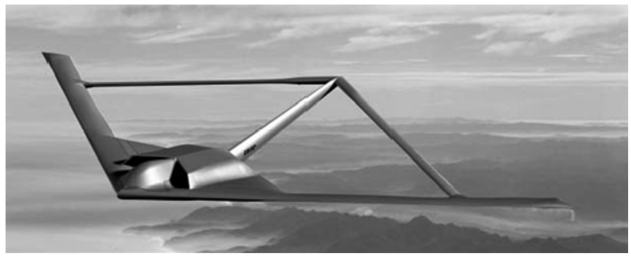

Fig. 2 Boeing sensor-craft concept.

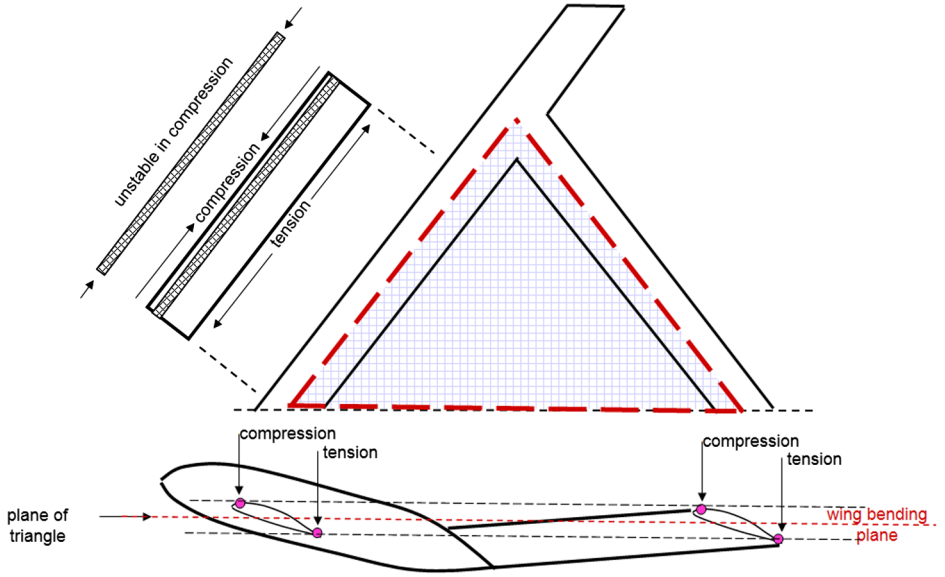

Fig. 3 Joined-wing bending plane.

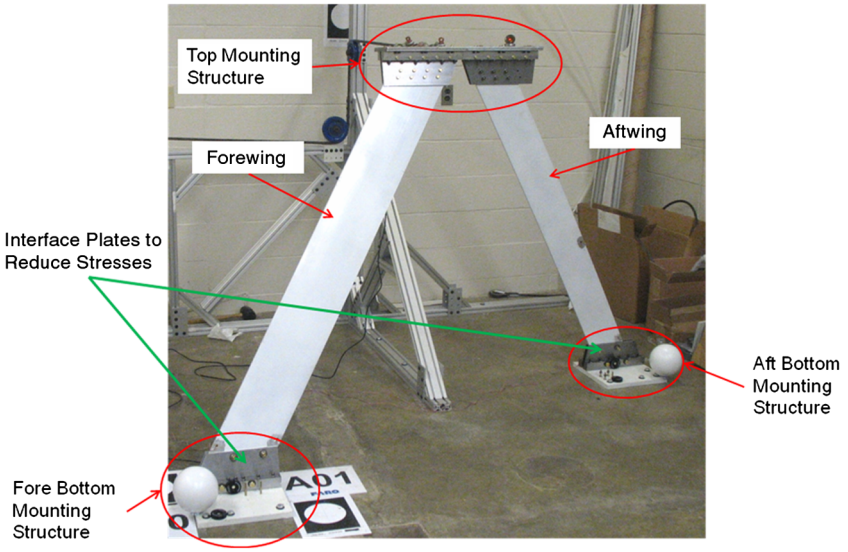

Fig. 4 2 m joined-wing test article.

dimensions of $\frac{1}{2}$ by 8 in. for the forewing and 6 in. for the aftwing. All attachment fixtures are made of hardened 4130 tool steel to maximize safety and minimize motion at the wing root attachment points attached to the concrete floor. Besides approximating the geometric layout of the joined-wing configuration, the original primary design focus for static testing was the inclusion of a nonlinear bend–twist couple without permanent deformation of the test article.

For modal testing, a Polytec PSV-400-3D scanning laser Doppler vibrometer (LDV) was used to collect operational deflection shapes, natural frequencies, and damping ratios.

IV. Finite Element Model

Three distinct FEMs, each composed of nearly all beam, plate, and solid elements, of the 2 m joined-wing test article were originally created. The predominantly plate element model has almost 60,000 DOFs (see Fig. 5) and yielded the best results in terms of minimal model complexity and agreement between the measured and predicted static displacements. The hardened steel mounting and joint structures are modeled as well, while the concrete is assumed to be a rigid constraint. Connections between all plates are represented with rigid-link and 6-DOF spring elements. The 6-DOF spring elements allow a less than rigid connection between components. The values of these stiffnesses were initially selected [2] to match experimentally measured static deflections. The stiffnesses of the spring elements of the connection between the wings and the bottom mounting structures were tuned a second time[¶] to provide a closer fit of the first natural frequency with its measured counterpart. This model, without any further tuning, was considered as the baseline model discussed in the previous section and led to natural frequencies shown in Table 1 and mode shapes as depicted in Fig. 6 [projected on the laser direction; see discussion of Eq. (11)].

V. Experimental Procedure

Figure 5 shows the 252 measurement locations as dots on the structure. These points were scanned using the Polytec PSV-400-3D scanning LDV. The joined-wing test article was excited with an autoping hammer with a force sensor mounted to the tip of the stinger. The excitation location remained fixed for all tests. Frequency response functions (FRFs) were computed for all measurement locations after 10 averages. The 252 FRFs collected were spectrally sieved around the resonance peaks, and a modal parameter estimation program (MEscope) was used to extract

[¶]Personal communication with B. Grier and R. Figliola, 2010.

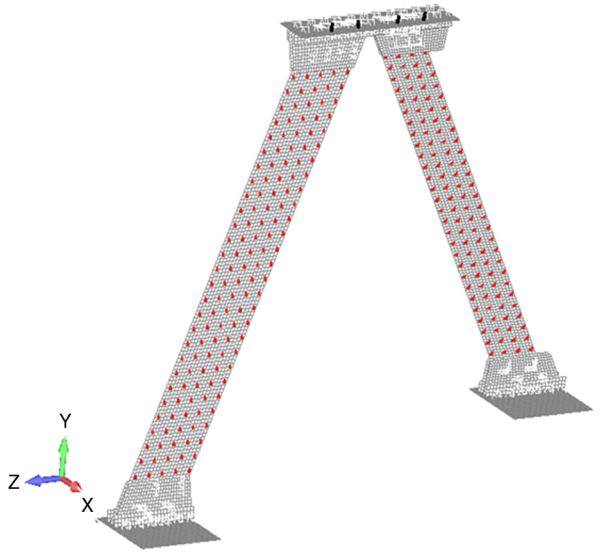

Fig. 5 2 m joined-wing FEM. Dots represent the 252 measurement locations that are coincident with the FEM nodes.

accurate estimates of the mode shapes, natural frequencies, and modal damping factors. Note that the extracted mode shapes were complex, although very close to purely imaginary for the points with significant motion. Thus, the imaginary parts and absolute values of the modes could both be used as estimates of the mode shapes. A third set of such estimates was obtained using the Niedbal approach [25], in which the complex-valued modal matrix Ψ_C (the columns of which are the estimated complex modes) is transformed into a real-valued one Ψ_N according to

$$\Psi_N = Re(\Psi_C) + Im(\Psi_C)[Re(\Psi_C)^T Re(\Psi_C)]^{-1} Re(\Psi_C)^T Im(\Psi_C) \tag{10}$$

A. Structural Population

A key in the present effort is the availability of test data on different structures for the estimation of the level of structural uncertainty. As a first validation of the proposed concepts and methods, it was decided to simulate the variability in structures by disassembling and reassembling the wings. In this process, the 22 bolts of the top plate of the top mounting structure were first removed, releasing the two wings, which were separated from each other by 6 mm. Then, these two wings were brought back together, the top plate was reinserted, and the 22 bolts were refastened to the specified torque.

The testing described in the previous subsection was first performed on the wing in the configuration that it was left in after the testing reported in [2]. To obtain an assessment of the variability in the measurement and data analysis process, three repeat tests were carried out on that structure (referred to as structure 1 in the remainder of this paper) without any disassembly. The extracted natural frequencies are given in Table 1 (columns labeled Repeat 1, Repeat 2, and Repeat 3). The disassembly and reassembly processes were then carried out three times to obtain structures 2, 3, and 4, which were each tested as described previously but only once; see Table 1 for the corresponding natural frequencies and Fig. 6 for the mode shapes of structure 4.

B. Modal Projection on the Finite Element Basis

The first step in the estimation of the mean matrix $\overline{K}$ and uncertainty parameter λ is the projection of the experimental mode shapes on the FE basis [see Eq. (4)] and the selection of the number N of such modes to be included in the basis. In this regard, it must first be noted that a single laser vibrometer was used in the experimental setup; thus, the mode shapes identified correspond, in fact, to the three-dimensional modal deflections projected along the direction of the laser beam, from the collimator to the measurement point. To maintain consistency in the estimation of the coefficients $\alpha_{mj}^{(r)}$, the basis $\boldsymbol{\phi}_j$ was then constructed using a similar projection of the three-dimensional FE modes on the direction of the local direction of the laser beam. That is,

$$\phi_{j,i} = \boldsymbol{\phi}_{j,i}^{\text{FEM}} \cdot \frac{(\boldsymbol{s}_i - \boldsymbol{s}_L)}{\|\boldsymbol{s}_i - \boldsymbol{s}_L\|} \tag{11}$$

where $\phi_{j,i}$ and $\boldsymbol{\phi}_{j,i}^{\text{FEM}}$ are the components of the modal basis function and FE mode shape j corresponding to measurement point i of coordinate $\boldsymbol{s}_i$. Furthermore, $\boldsymbol{s}_L$ denotes the position vector of the laser collimator. The computations of Eq. (11) were carried out for FE modes 1, 2, 3, 4, 5, 7, etc. Mode 6 was not included in this list because it is predominantly in-plane (at the contrary of the others predominantly transverse) and because it was not observed experimentally in the band of interest (i.e., below 100 Hz).

The projection of the experimental mode shapes on the basis $\boldsymbol{\phi}_j$ (see Fig. 6 for structure 4) was next carried out for repeat 3 of structure 1 and the measurements of structures 2–4 for an increasing number N of transverse-dominant basis functions, and the overall error [see Eq. (5)] was determined in each case. The evolution of this error with N is shown in Fig. 7 and suggests that the use of $N = 6$ FE modes (modes 1, 2, 3, 4, 5, and 7) allows the error to reach its noise-related floor. Note that, in Fig. 7, experimental mode 5 was not used in the computation of the error because it is significantly more noisy than the other modes owing to the accidental coincidence of its natural frequency with the 60 Hz electric power frequency. The inclusion of this mode in the error raises significantly the noise floor level and renders more difficult the capturing of the convergence of the error. Note finally that the results presented in Fig. 7 were obtained with the experimental mode shapes estimated by all three methods: imaginary part, absolute of the complex mode, and Niedbal transformation [25]; see Eq. (10). The first two provide errors that are almost exactly equal, while the latter gives a very slightly larger value. In all ensuing discussions, the imaginary part of the complex mode was used.

With the number of basis functions and the coefficients $\alpha_{mj}^{(r)}$ estimated, it is possible to form reconstructed mode shapes, i.e., the projections of the experimental ones on the basis as expressed by the right-hand side of Eq. (4). These modes are also shown in Fig. 6 for the experimental data of structure 4. The modal assurance criterion (MAC) values of the experimental data (imaginary part of the complex modes) with the corresponding basis function (FE mode projected on the laser direction) and with the reconstructed mode

Table 1 Natural frequencies (Hz) obtained from the FEM and experimentally measured[a]

	FEM	Repeat 1	Repeat 2	Repeat 3	Struct. 2	Structure 3	Structure 4
1	8.30	8.33	8.31	8.30	8.26	8.29	8.27
2	16.09	15.33	15.38	15.37	14.95	15.03	15.00
3	19.50	20.61	20.58	20.58	20.54	20.58	20.58
4	33.64	38.08	38.07	38.05	37.70	37.74	37.07
5	55.45	60.04	59.97	59.96	59.98	59.92	59.88
6	73.93	>100	>100	>100	>100	>100	>100
7	75.51	88.37	88.55	88.50	86.03	86.22	80.50

[a]Repeats 1, 2, and 3 denote three tests of structure 1.

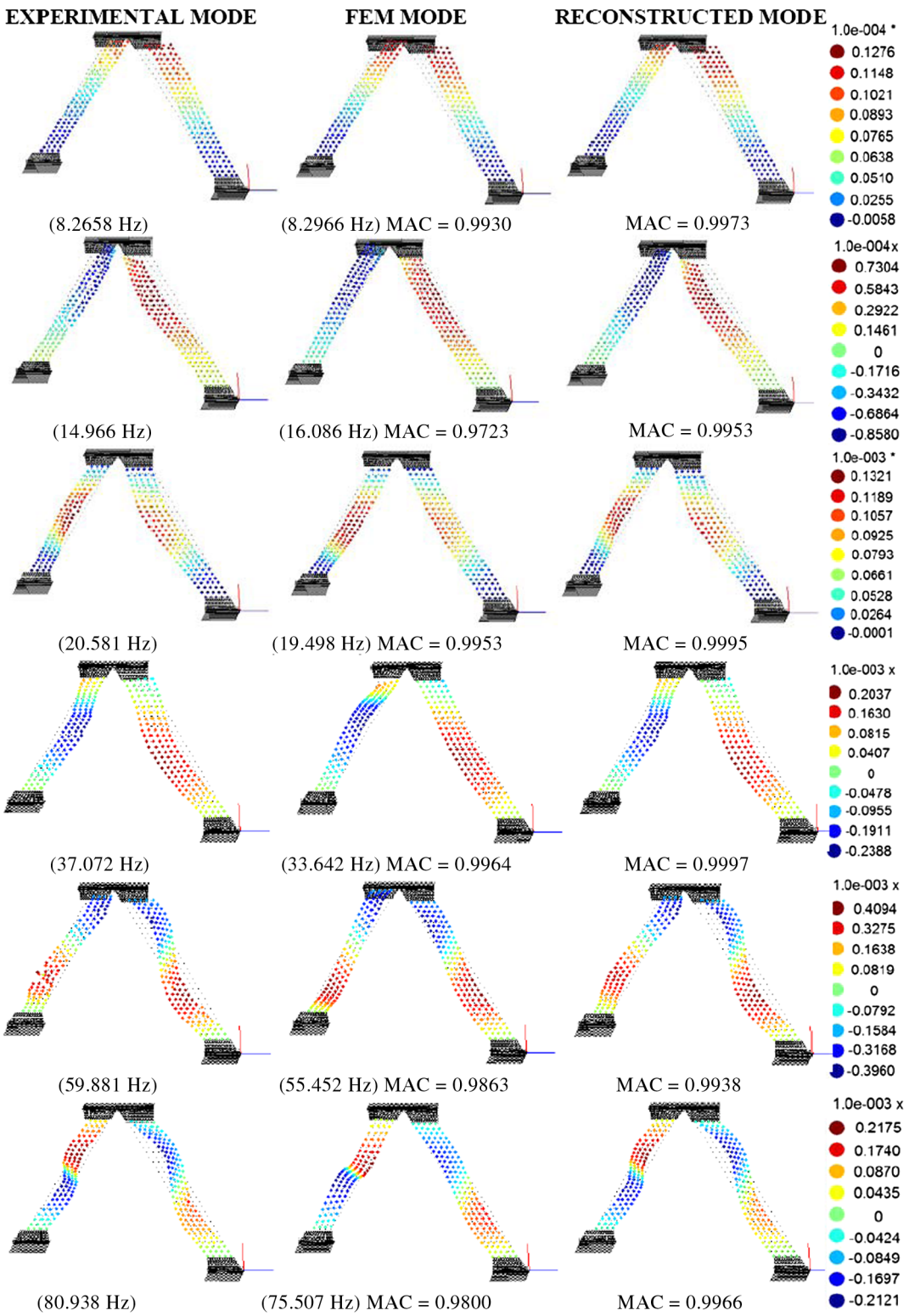

Fig. 6 Experimental mode shapes (imaginary part estimate), laser projected FE mode shapes, and experimental mode shapes projected in the basis.

shapes are also presented on Fig. 6. The high values (greater than or equal to 0.972) of the former MAC (between experiment and basis functions) demonstrate the good accuracy of the FEM (even though there are notable discrepancies on natural frequencies; see Table 1) and the low level of noise in the laser data. After reconstruction, the MAC values are even higher (greater than or equal to 0.993), clearly confirming the adequacy of the basis for the representation of the experimental mode shapes and the presence of a slight coupling between the basis functions.

This coupling can also be observed in the projection coefficients $\alpha_{mj}^{(r)}$, which are very close to 1 for $m = j$ and rather small for $m \neq j$; see Table 2 for structure 1, repeat 3 data, which is rather typical. A pictorial representation of these coefficients is shown in Fig. 8. Note from this figure and from Table 2 that the column associated with experimental mode 5 (of frequency very close to 60 Hz) involves larger coefficients $\alpha_{mj}^{(r)}$ for $m \neq j$, owing probably to the larger noise level on this mode.

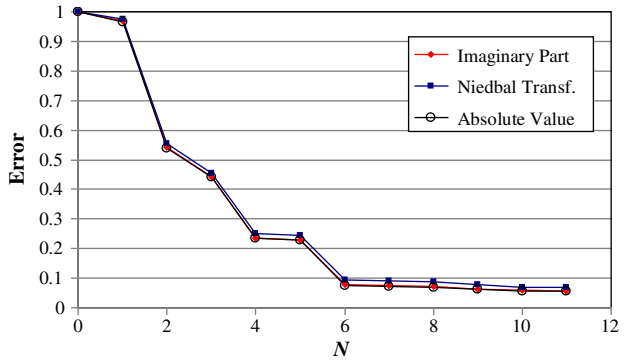

Fig. 7 Original projection error of Eq. (5) vs number of transverse-dominant basis functions. Experimental modes 5 and 6 not used. Mode shape selected from imaginary part, absolute value of the complex mode, or through the Niedbal transformation.

VI. Mean Model and Uncertainty Parameter Estimation

The estimation of the mean stiffness matrix $\overline{K}$ and uncertainty parameter λ from the measured natural frequencies and projection coefficients $\alpha_{mj}^{(r)}$ according to the maximum likelihood approach is estimated with a base of six FEM modes.

A. Optimization Algorithm Specificities

As can be seen from Eqs. (6–9), the evaluation of the likelihood function requires the determination of the mean vector $\boldsymbol{\mu}_X(\overline{K}, \lambda)$ and the covariance matrix $K_{XX}(\overline{K}, \lambda)$. Yet, neither one can be determined in closed-form expression; thus, it is necessary to proceed with a Monte Carlo simulation. Let S be the number of random stiffness matrices simulated for a particular mean matrix $\overline{K}$ and uncertainty parameter λ. For each of these matrices, an eigenvalue computation is carried out and yields a vector $\boldsymbol{X} = \boldsymbol{X}^{(s)}$ composed of the natural frequencies and mode shape values. Then, the mean $\boldsymbol{\mu}_X$ of this vector can be estimated from the population of size S as

$$\boldsymbol{\mu}_X \approx \frac{1}{S}\sum_{s=1}^{S} \boldsymbol{X}^{(s)} \tag{12}$$

The covariance matrix is similarly estimated from the samples $\boldsymbol{X}^{(s)}$ as

$$K_{XX} \approx \frac{1}{S-1}\sum_{s=1}^{S} (\boldsymbol{X}^{(s)} - \boldsymbol{\mu}_X)\,(\boldsymbol{X}^{(s)} - \boldsymbol{\mu}_X)^T \tag{13}$$

Because of the finiteness of the number of samples S, Eqs. (12) and (13) only provide estimates of the true mean and covariance matrix. Furthermore, these estimates are random; they vary from one population of S samples to another exhibiting a standard deviation that is typically of the order of $1/\sqrt{S}$.

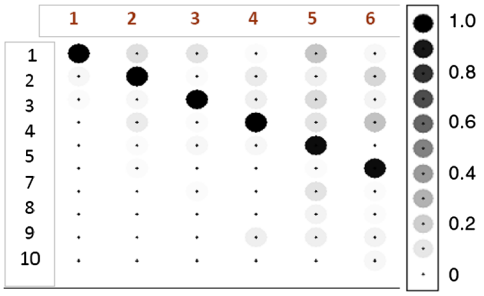

Fig. 8 Projection coefficients $\alpha_{mj}^{(r)}$ for structure 1, repeat 3.

Thus, if a perturbation Δ in either $\overline{K}$ or λ is performed, corresponding changes in $\boldsymbol{\mu}_X(\overline{K}, \lambda)$ and $K_{XX}(\overline{K}, \lambda)$ are obtained that are composed of two parts. The first component is the change in the true value of the mean vector and covariance matrix that is implied by Δ. The second part, however, is a random term that results from the finiteness of S and the approximate nature of Eqs. (12) and (13). This latter term renders difficult the accurate evaluation of gradients, especially when they are close to zero, unless the sample size S is taken to be prohibitively large.

These observations demonstrate that the numerical optimization of the likelihood function should be accomplished by relying on methods that do not need gradient evaluation, as is necessary when the objective function is not smooth. In this effort, pattern search and simulated annealing methods were employed for finding the maximum of the likelihood function. In fact, simulated annealing was found to perform better in finding the best (global) optimum than pattern search did.

A second specificity of the current optimization problem concerns the mean stiffness matrix $\overline{K}$. Indeed, it is necessary that this matrix remains positive definite and symmetric. While the latter property is easily built in, the former is not. Imposing the positiveness of the eigenvalues of $\overline{K}$ leads to algorithmic difficulties, and an alternative formulation is desired. The constrained optimization can be recast into an unconstrained one by varying, not the components of $\overline{K}$ but rather the components of the lower triangular matrix $\overline{L}_K$ corresponding to the Cholesky decomposition of $\overline{K}$, i.e., with

$$\overline{K} = \overline{L}_K \overline{L}_K^T \tag{14}$$

In fact, this decomposition is necessary in the nonparametric modeling effort. Note that the results presented herein were obtained with a slightly different formulation in which the mean stiffness matrix is expressed as would be obtained from its eigenvalues and eigenvectors, i.e., as

$$\overline{K} = Q \cdot \Lambda \cdot Q^T \tag{15}$$

where Λ is diagonal with positive elements.

Table 2 Projection coefficients $\alpha_{mj}^{(r)}$ for structure 1, repeat 3

	Experimental modes					
Basis function	1	2	3	4	5	7
1	0.9989	−0.1340	0.1159	0.0310	0.2200	0.0455
2	−0.0386	−0.9861	0.0289	−0.0889	−0.0750	−0.1695
3	0.0236	0.0358	−0.9911	0.0758	0.1475	0.0576
4	−0.0093	0.0793	−0.0245	−0.9899	0.1202	0.2432
5	0.0065	0.0266	0.0467	0.0343	−0.9421	0.0001
6	0.0023	0.0304	0.0016	−0.0035	0.0173	−0.9493
7	−0.0047	0.0074	−0.0266	0.0011	−0.1180	−0.0227
8	0.0050	0.0075	0.0020	−0.0113	0.0547	0.0234
9	0.0015	0.0117	−0.0022	0.0636	0.0707	0.0574
10	−0.0015	0.0135	−0.0021	−0.0116	0.0061	−0.0362

B. Normalization

Numerical difficulties/instabilities were encountered in the optimization process when the uncertainty level was small (i.e., large λ) and which were traced to the small values of the elements of the covariance matrix. This issue can be eliminated by appropriately renormalizing the variables. Specifically, proceed first with the Cholesky decomposition of the covariance matrix as

$$K_{XX} = VV^T \tag{16}$$

Next, introduce the new random variables:

$$Y = V^{-1}(\boldsymbol{X} - \boldsymbol{\mu}_X) \tag{17}$$

Then, proceeding with the change of random variables leads to

$$p_Y^G(y; \overline{K}, \lambda) = \frac{1}{(2\pi)^{p/2}} \exp\left[-\frac{1}{2} \cdot \boldsymbol{y}^T \boldsymbol{y}\right] \tag{18}$$

since the covariance matrix K_{YY} is readily shown to be identity.

C. Likelihood Function Versus Log-Likelihood Function

Rewriting the likelihood function in terms of the variables $\boldsymbol{Y}$ leads to

$$L = \prod_{r=1}^{R} p_Y(\boldsymbol{y}^{(r)}; \overline{K}, \lambda) \frac{1}{\det(V)} = \prod_{r=1}^{R} p_Y(\boldsymbol{y}^{(r)}; \overline{K}, \lambda) \frac{1}{\sqrt{\det(K_{XX})}} \tag{19}$$

Occasionally, small values of the probability density function are obtained that can result in numerical difficulties (underflow). This issue is resolved by proceeding with the maximization of the log-likelihood function $\log(L)$, which is obtained as

$$\log(L) = \sum_{r=1}^{R} \left(\log\left(\frac{1}{(2\pi)^{p/2} \cdot \sqrt{\det(K_{XX})}} \right) - \frac{1}{2} \boldsymbol{y}^T \boldsymbol{y} \right) \tag{20}$$

D. Orthogonality of Modes

The mode shapes simulated on the basis of the nonparametric model correspond to a symmetric eigenvalue problem and are thus orthogonal with respect to both mass and stiffness matrices. In the present effort, the modal basis was formed from mass normalized mode shapes; thus, the mean (constant) mass matrix of the reduced-order model is identity. Thus, all simulated values $\alpha_{mj}^{(r)}$ satisfy the orthogonality condition

$$A^{(r)T} A^{(r)} = I \tag{21}$$

where $A^{(r)}$ is the matrix of the coefficients $\alpha_{mj}^{(r)}$. Such a property is in general not satisfied by the experimental measurements because of noise and differences between the real structure and the computational model. This lack of consistency between the properties of the simulated and experimental modes was found to be a significant problem in the reliable estimation of the uncertainty parameter λ or equivalently of δ defined as

$$\delta^2 = \frac{n+1}{n+2\lambda-1} \tag{22}$$

The orthogonality condition existing on the simulated mode shapes implies, in fact, that the coefficients $\alpha_{mj}^{(r)}$ cannot be independent of each other. In fact, note that the matrices $A^{(r)}$ are very close to the identity matrix for a small level of uncertainty; that is, they can be expressed as

$$A^{(r)} = I + \Delta A^{(r)} \tag{23}$$

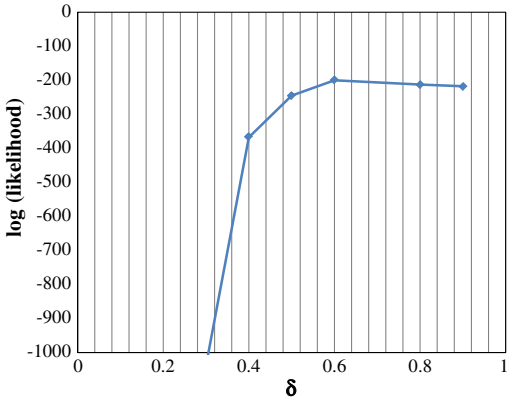

Fig. 9 Maximum value of the log-likelihood as a function of uncertainty level (δ), original method.

From the orthogonality property, one concludes that $[A^{(r)}]^{-1} = A^{(r)T}$ or

$$[I + \Delta A^{(r)}]^{-1} = [I + \Delta A^{(r)}]^T = I + \Delta A^{(r)T} \tag{24}$$

Using a Neumann expansion for small $\Delta A^{(r)}$, i.e., such that all of its eigenvalues are significantly less than 1 in magnitude, one obtains

$$[I + \Delta A^{(r)}]^{-1} \approx I - \Delta A^{(r)} \tag{25}$$

Comparing, finally, Eqs. (24) and (25) leads to

$$\Delta A^{(r)T} = -\Delta A^{(r)} \tag{26}$$

which demonstrates that $\Delta A^{(r)}$ is skew symmetric because of the orthogonality condition when the uncertainty level is small. While this property does not hold for larger uncertainty levels, the preceding derivation nevertheless demonstrates that there is a strong relation between the upper and lower triangular elements of $\Delta A^{(r)}$; thus, only one of these two groups should be considered independent variables.

In this light, the likelihood function was not built on the distribution of the entire set of coefficients $\alpha_{mj}^{(r)}$, $j = 1, \ldots, N-1$,

$$\beta_{mj} = \begin{bmatrix} 0 & & & & & \\ -0.0396 & 0 & & & & \text{skew-symmetric} \\ -0.0073 & 0.0132 & 0 & & & \\ -0.0379 & 0.0633 & -0.0636 & 0 & & \\ 0.0819 & 0.0855 & 0.0621 & -0.0496 & 0 & \\ 0.0671 & 0.0466 & 0.0034 & -0.0697 & -0.0225 & 0 \end{bmatrix}$$

a)

$$\beta_{mj} = \begin{bmatrix} 0 & & & & & \\ 0.0689 & 0 & & & & \text{skew-symmetric} \\ -0.0288 & 0.0005 & 0 & & & \\ -0.0552 & 0.0296 & -0.0585 & 0 & & \\ 0.1579 & 0.0270 & 0.0848 & -0.014 & 0 & \\ 0.0753 & 0.0592 & 0.0235 & -0.0554 & 0.0028 & 0 \end{bmatrix}$$

b)

$$\text{std}\left[\beta_{mj}^{(r)}\right] = \begin{bmatrix} 0 & & & & & \\ 0.084 & 0 & & & & \text{symmetric} \\ 0.0429 & 0.0345 & 0 & & & \\ 0.0245 & 0.0131 & 0.0076 & 0 & & \\ 0.0529 & 0.0729 & 0.0328 & 0.0692 & 0 & \\ 0.0439 & 0.0432 & 0.0189 & 0.0541 & 0.017 & 0 \end{bmatrix}$$

c)

Fig. 10 Representations of a–b) values of β_{mj} obtained in the first and third tests, and c) standard deviations of the random coefficients $\beta_{mj}^{(r)}$.

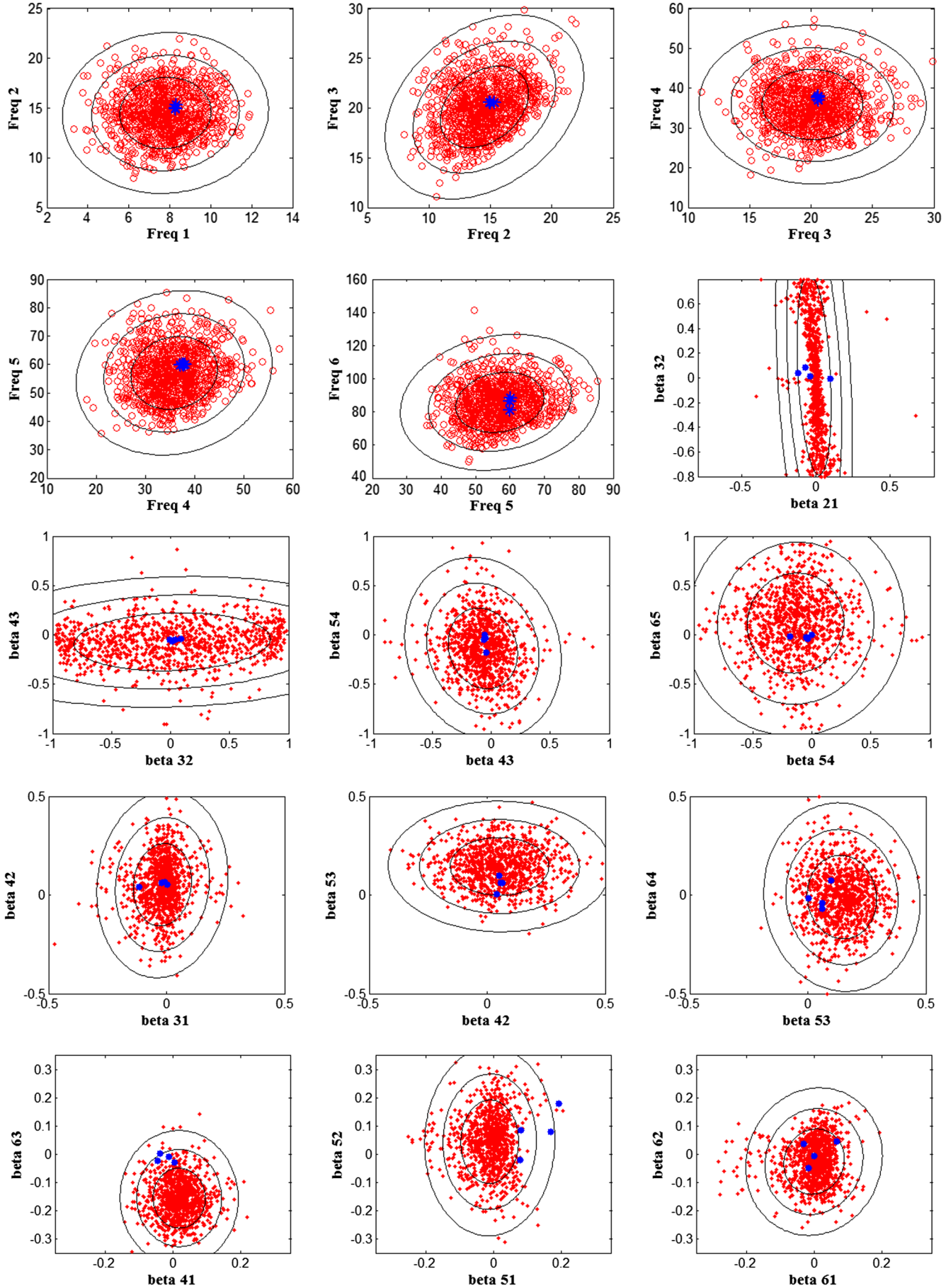

Fig. 11 Two-dimensional joint probability density functions of the natural frequencies (freq) and $\beta_{mj}^{(r)}$ values, original method.

$m = 1, \ldots, N$, as suggested by Eqs. (6–8) but rather of the combinations

$$\beta_{mj} = [\alpha_{mj}^{(r)} - \alpha_{jm}^{(r)}]/2 \quad \text{for } j = 1, \ldots, m-1, m = 2, \ldots, N \quad (27)$$

Using this set of variables and the orthogonality conditions of Eq. (21), the entire matrix $A^{(r)}$ can be uniquely built. Thus, the use of the set $[\alpha_{mj}^{(r)} - \alpha_{jm}^{(r)}]/2$ takes automatically into account the orthogonality constraints, which thus need not be considered any further.

E. Effect of Noise and Modal Coupling

The preceding optimization process was applied to the joined-wing data. The initial condition used for the mean stiffness matrix $\overline{K}$ was selected as the matrix for which the eigenvalues are the squared frequencies average over the tests considered and with mode shapes similarly averaged from the matrices A. Furthermore, the optimization process was carried out for a set of fixed values of the uncertainty parameter (λ or δ) and the resulting maximum value of the log-likelihood function was determined for each uncertainty level. Collecting these results led to the plot of Fig. 9, which shows that the highest value of the likelihood function is obtained for a rather large uncertainty level, i.e., $\delta = 0.6$.

This optimum value of the uncertainty level appears significantly larger than would have initially been expected from the natural frequencies. The spread in these values seems consistent with a value of $\delta = 0.1$ or less. This contradiction suggests that the high uncertainty level estimated results from some peculiarity of the test data mode shapes. To obtain a better perspective on this situation, shown in Fig. 10 are the values of β_{mj} obtained in the first and third tests, as representative examples, as well as the standard deviation of these values obtained from the nonparametric approach with an uncertainty level of $\delta = 0.3$.

An inspection of the test values of Figs. 10a and 10b in comparison with the standard deviations of Fig. 10c demonstrate that there are a few outliers in the data, i.e., values that exceed the three standard deviations threshold. Clearly, the maximum likelihood method will be biased by these values and will tend to increase the level of uncertainty in the system until these outliers have a higher probability level. An equivalent perspective can be drawn from the plots of Fig. 11, which provide a series of two-dimensional joint probability density functions of the natural frequencies and $\beta_{mj}^{(r)}$ values.

Plotted on these figures are 1) the test points (as large stars), 2) one-, two-, and three-standard-deviation contour lines [which are ellipses according to the approximate Gaussian distribution of Eq. (8); shown as lines], and 3) a series of simulated values of the frequencies and $\beta_{mj}^{(r)}$ values (as small circles). The presence of the outliers is clearly shown as well on these plots.

Among the outliers, one recognizes particularly the terms (5,1), (5,2), (6,1), and (6,2), and these components surface as outliers in particular because of the small values of the corresponding standard deviations. In fact, an inspection of Fig. 10c reveals that the standard deviations are at a maximum between modes of consecutive natural frequencies and steadily decrease as the separation between natural frequencies increases.

Why then are some of these β_{mj} values so large? Those associated with mode 5 can easily be dismissed as noise related. Indeed, the natural frequency of this mode is almost exactly 60 Hz, and a strong presence of the power frequency in the response was observed at the time of the test. Accordingly, a good practice would be not to involve this mode in the computations. This argument then leaves the (6,1) and (6,2) components. The former component may exhibit a trend, being large in the last three tests and of the same sign. The latter one, however, appears only in the last test. Since the values of these coefficients β_{mj} are not exceedingly large, it is indeed possible that noise is still responsible for the issue.

To address the presence of the outliers, two different efforts were carried out in this investigation. First, the modeling procedure was repeated without mode 5 to eliminate the effect of the noise implied by the coincidence of its natural frequency with the power frequency. This process did not lead to a significant change in the optimum value of δ, most likely because of the remaining presence of the (6,1) and (6,2) components; see Fig. 12.

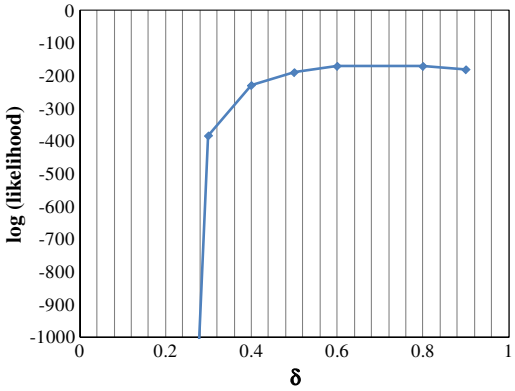

Fig. 12 Maximum value of the log-likelihood as function of the uncertainty level (δ): original method without mode 5.

A second effort focused on reformulating the projection of the test mode shapes on their FE counterparts to minimize the effect of noise. This revised formulation is described next.

F. Revised Projection Formulation

The determination of the projection coefficients α_{mj} has been performed up to this point to minimize the representation error

$$E_{\text{rep}}^{(m)} = \left\| \boldsymbol{\psi}_m^{(r)} - \sum_{j=1}^{N} \alpha_{mj}^{(r)} \boldsymbol{\phi}_j \right\|^2 \quad (28)$$

for each mode m of test r. If noise is present in the mode shape measurements, it will be modeled as part of the test mode and will be present in the ensuing computations, potentially biasing the maximum likelihood identification strategy toward a higher uncertainty level.

In this light, it would be desirable to filter out the noise, i.e., to fine-tune the estimation of the coefficients α_{mj} toward their use in the nonparametric modeling effort. As in the original projection-based determination of the coefficients α_{mj}, this process will be accomplished mode per mode and test per test. For a given mean model $\overline{K}$ and uncertainty level λ, the fitness of a set of coefficients α_{mj} can be assessed through the discrepancy measure

$$F_m^{(r)} = \sum_{j}^{N} \frac{(\alpha_{mj} - \bar{\alpha}_{mj})^2}{\sigma_{mj}^2} \quad (29)$$

where $\bar{\alpha}_{mj}$ and σ_{mj} are the mean and standard deviations of the random mode shapes A_{mj} obtained with $\overline{K}$ and λ. The larger $F_m^{(r)}$ is, the less fit the coefficients α_{mj} are for nonparametric modeling or, equivalently, the larger the corresponding uncertainty level will be. Accordingly, it is desired to minimize $F_m^{(r)}$. However, this

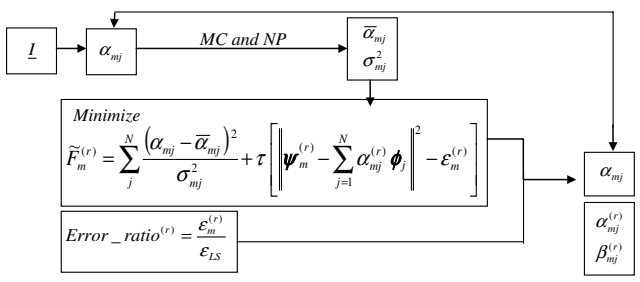

Fig. 13 Iterative process to obtain the projection coefficients, revised formulation (MC denotes Monte Carlo, and NP denotes nonparametric model).

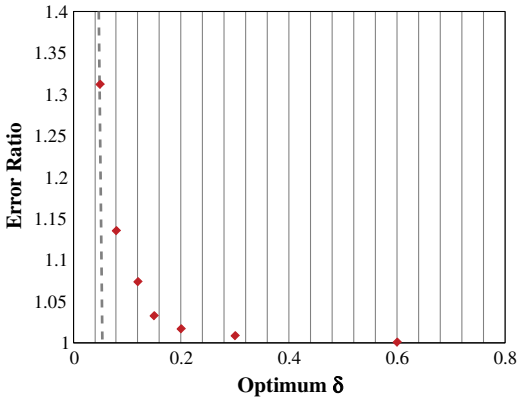

Fig. 14 Optimum δ values corresponding to various error ratios ρ, revised formulation.

discrepancy measure does not involve the measured mode $\boldsymbol{\psi}_m^{(r)}$, and thus cannot be used by itself. In fact, it is necessary that the coefficient α_{mj} that minimizes $F_m^{(r)}$ also provides a good representation of the mode shape $\boldsymbol{\psi}_m^{(r)}$. This requirement will be achieved by constraining the optimization of $F_m^{(r)}$ to give a small representation error; that is,

$$\left\| \boldsymbol{\psi}_m^{(r)} - \sum_{j=1}^{N} \alpha_{mj}^{(r)} \boldsymbol{\phi}_j \right\|^2 = \varepsilon_m^{(r)} \tag{30}$$

To impose the value $\varepsilon_m^{(r)}$, it is useful to first determine its smallest value $\bar{\varepsilon}_m^{(r)}$, which is obtained by minimizing $E_{\text{rep}}^{(m)}$ [Eq. (28)]. In fact, $\bar{\varepsilon}_m^{(r)}$ is the representation error obtained with the original projection approach to determine the coefficients α_{mj}. Accordingly, it is proposed here to set $\varepsilon_m^{(r)} = \rho\, \bar{\varepsilon}_m^{(r)}$, where ρ is a user-selected ratio greater than or equal to 1.

The minimization of $F_m^{(r)}$ [Eq. (29)] under the representation constraint of Eq. (30) can be achieved by the Lagrange multiplier (denoted here as τ) approach, i.e., with the unconstrained minimization of

$$\tilde{F}_m^{(r)} = \sum_{j}^{N} \frac{(\alpha_{mj} - \bar{\alpha}_{mj})^2}{\sigma_{mj}^2} + \tau \left[\|\boldsymbol{\psi}_m^{(r)} - \sum_{j=1}^{N} \alpha_{mj}^{(r)} \boldsymbol{\phi}_j\|^2 - \varepsilon_m^{(r)} \right] \tag{31}$$

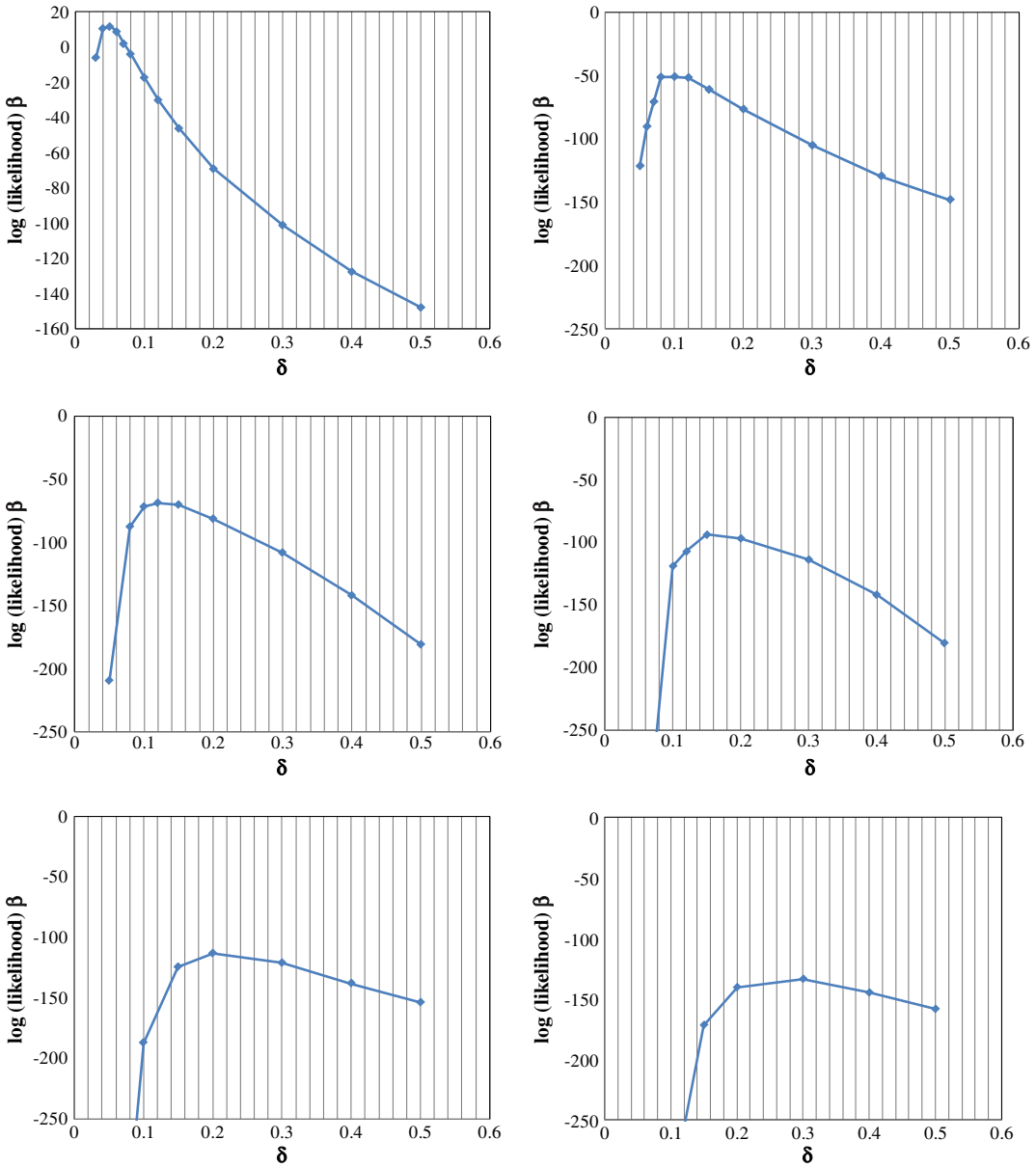

Fig. 15 Maximum value of the log-likelihood as a function of the uncertainty level (δ) for various error ratios (ρ): a) $\rho = 1.31$, b) $\rho = 1.17$, c) $\rho = 1.07$, d) $\rho = 1.03$, e) $\rho = 1.016$, and f) $\rho = 1.008$.

$$\boldsymbol{\beta} = \begin{bmatrix} 0 & 0.0022 & -0.0152 & 0.0026 & -0.0022 & -0.0006 \\ -0.0022 & 0 & -0.0342 & 0.0079 & 0.0018 & 0.0012 \\ 0.0152 & 0.0342 & 0 & -0.0688 & 0.0050 & -0.0027 \\ -0.0026 & -0.0079 & 0.0688 & 0 & -0.0177 & -0.0166 \\ 0.0022 & -0.0018 & -0.0050 & 0.0177 & 0 & -0.0640 \\ 0.0006 & -0.0012 & 0.0027 & 0.0166 & 0.0640 & 0 \end{bmatrix}$$

$$\boldsymbol{\beta} = \begin{bmatrix} 0 & 0.0306 & -0.0106 & 0.0035 & -0.0002 & 0.0014 \\ -0.0306 & 0 & -0.1002 & 0.0021 & 0.0008 & -0.0003 \\ 0.0106 & 0.1002 & 0 & -0.0481 & 0.0010 & 0.0016 \\ -0.0035 & -0.0021 & 0.0481 & 0 & -0.0182 & -0.0143 \\ 0.0002 & -0.0008 & -0.0010 & 0.0182 & 0 & -0.0319 \\ -0.0014 & 0.0003 & -0.0016 & 0.0143 & 0.0319 & 0 \end{bmatrix}$$

$$\boldsymbol{\beta} = \begin{bmatrix} 0 & 0.0344 & -0.0126 & 0.0035 & -0.0012 & -0.0003 \\ -0.0344 & 0 & -0.1359 & 0.0006 & 0.0025 & -0.0017 \\ 0.0126 & 0.1359 & 0 & -0.0655 & 0.0006 & 0.0016 \\ -0.0035 & -0.0006 & 0.0655 & 0 & -0.0410 & -0.0207 \\ 0.0012 & -0.0025 & -0.0006 & 0.0410 & 0 & -0.0663 \\ 0.0003 & 0.0017 & -0.0016 & 0.0207 & 0.0663 & 0 \end{bmatrix}$$

$$\boldsymbol{\beta} = \begin{bmatrix} 0 & -0.0025 & -0.0052 & 0.0015 & 0.0006 & 0.0026 \\ 0.0025 & 0 & 0.0926 & 0.0140 & 0.0022 & 0.0020 \\ 0.0052 & -0.0926 & 0 & -0.0143 & -0.0065 & -0.0070 \\ -0.0015 & -0.0140 & 0.0143 & 0 & -0.0362 & -0.0020 \\ -0.0006 & -0.0022 & 0.0065 & 0.0362 & 0 & -0.0230 \\ -0.0026 & -0.0020 & 0.0070 & 0.0020 & 0.0230 & 0 \end{bmatrix}$$

$$\boldsymbol{\beta} = \begin{bmatrix} 0 & 0.0072 & -0.0081 & 0.0030 & -0.0004 & 0.0003 \\ -0.0072 & 0 & -0.0189 & 0.0085 & -0.0002 & -0.0043 \\ 0.0081 & 0.0189 & 0 & -0.0565 & 0.0048 & -0.0027 \\ -0.0030 & -0.0085 & 0.0565 & 0 & -0.0181 & -0.0204 \\ 0.0004 & 0.0002 & -0.0048 & 0.0181 & 0 & -0.0506 \\ -0.0003 & 0.0043 & 0.0027 & 0.0204 & 0.0506 & 0 \end{bmatrix}$$

$$\boldsymbol{\beta} = \begin{bmatrix} 0 & 0.0276 & -0.0086 & 0.0023 & -0.0004 & -0.0002 \\ -0.0276 & 0 & -0.0778 & 0.0135 & 0.0071 & -0.0021 \\ 0.0086 & 0.0778 & 0 & -0.0557 & 0.0026 & -0.0025 \\ -0.0023 & -0.0135 & 0.0557 & 0 & -0.0072 & -0.0036 \\ 0.0004 & -0.0071 & -0.0026 & 0.0072 & 0 & -0.0926 \\ 0.0002 & 0.0021 & 0.0025 & 0.0036 & 0.0926 & 0 \end{bmatrix}$$

Fig. 16 Values of β_{mj} obtained in the six tests. Error ratio $\rho = 1.31$.

Differentiating the preceding expression with respect to α_{mj} leads to the system of equations

$$[\Sigma + \tau \Phi^T \Phi]\, \boldsymbol{A}_m^{(r)} = \tau\, \Phi^T \boldsymbol{\psi}_m^{(r)} + \Sigma \bar{\boldsymbol{A}}_m \tag{32}$$

where Σ is the diagonal matrix with element jj equal to $1/\sigma_{mj}^2$. Furthermore, Φ is the matrix with the vector $\boldsymbol{\phi}_j$ as the jth column, and $\boldsymbol{A}_m^{(r)}$ and $\bar{\boldsymbol{A}}_m^{(r)}$ are the vectors of coefficients α_{mj}, and $\bar{\alpha}_{mj}$.

The solution of the linear system of equations of Eq. (32) yields $\boldsymbol{A}_m^{(r)}$ in terms of the yet unknown Lagrange multiplier τ. Then, introducing this result in Eq. (30) leads to a nonlinear algebraic equation for τ in terms of the allowed error $\varepsilon_m^{(r)}$. Once solved, the value of τ can be reintroduced in $\boldsymbol{A}_m^{(r)}$ to yield the final expression for the coefficients α_{mj}.

It should be noted that this revised approach is an extension/generalization of the original projection method described before. Indeed, if one sets $\varepsilon_m^{(r)} = \bar{\varepsilon}_m^{(r)}$, the previous set of coefficients $\varepsilon_m^{(r)}$ is recovered and the value of τ is $\propto$.

Implicit in the preceding formulation is the knowledge of the mean matrix $\overline{K}$ and the uncertainty level λ that is necessary for the evaluation of $\bar{\alpha}_{mj}$ and σ_{mj}. Certainly, an iterative scheme could be developed in which an initial estimate of $\bar{K}$ and λ is used, and then the process could be updated and repeated until convergence. In this regard, note however that the mean values $\bar{\alpha}_{mj}$ remain very close to δ_{mj} (the Kronecker symbol), even for large uncertainty (small λ), and thus could be set in this fashion. Furthermore, it was found by experimenting with the nonparametric approach that the standard deviations σ_{mj} all grow approximately proportionally as the level of uncertainty increases, except for the diagonal term that grows much slower. If one neglects this difference of the diagonal terms, it is found that the solution $\boldsymbol{A}_m^{(r)}$ is independent of an overall scaling of the matrix Σ, which would only be reflected in the value of the Lagrange multiplier τ. On the basis of this discussion, an iterative process may not be necessary and $\bar{\alpha}_{mj}$ and σ_{mj} may be set according to first estimates of the mean matrix $\overline{K}$ and the uncertainty level λ.

Notwithstanding these comments, the iterative process was implemented here to fully assess the methodology (see Fig. 13 for a flowchart) and a set of increasing values of the error ratio ρ were considered. As indicated in Fig. 14, the allowance of a slightly larger error permits a much better fit by the nonparametric methodology and the optimum value of δ that decreases rapidly toward the value expected from a fit of the natural frequencies alone; that is, as ρ changes from 1 to 1.31, the maximum of the likelihood function occurs for a value of δ, which decreases from 0.6 to 0.05 (Fig. 15). A study of the resulting values β_{mj} (not shown here for brevity) clearly demonstrates that the outliers highlighted before are becoming smaller, as desired, as the projection error is allowed to increase slightly.

These results demonstrate that the revised formulation achieves exactly the stated purpose, and thus is considered here as the projection approach for the identification of the maximum entropy-based uncertain model. But how should the error ratio be set? If no specific perspective is available to the analyst, the error should be set so that the value of δ obtained by the present process is consistent with the one that can be estimated from the natural frequencies alone, which was approximately 0.05 in the present case. Adopting this criterion leads to the error ratio $\rho = 1.31$, for which the final values β_{mj} are given in Fig. 16 and lead to the mean stiffness matrix $\overline{K}$ of Fig. 17.

It can be noted on the two-dimensional plots of Fig. 18 that mode 6 appears to have a larger deviation of natural frequencies than the other ones. On the basis of this observation, the modified nonparametric model introduced in [3] was also considered with a specific variance only on mode 6. As shown in Fig. 19, the ellipses corresponding to this mode have increased and the natural frequencies of mode 6 fit within these ellipses as the other modes.

All results described previously were obtained by relying on the Gaussian approximation of the joint probability density function of the random vector $\boldsymbol{X}$ [see Eq. (9)] to build the likelihood function of Eq. (6). Nevertheless, many of these computations were also repeated with the kernel density estimation method [11–13], using the Gaussian-based optimum solution as an initial condition, and only small variations in the parameters (mean stiffness matrix $\overline{K}$ and uncertainty parameter λ) were observed.

$$\overline{K} = \begin{bmatrix} 0.0323 & 0.0083 & -0.0062 & -0.0292 & 0.0483 & 0.0587 \\ 0.0083 & 0.0968 & 0.0021 & 0.0202 & 0.0903 & 0.0166 \\ -0.0062 & 0.0021 & 0.1685 & -0.0225 & 0.0195 & -0.0343 \\ -0.0292 & 0.0202 & -0.0225 & 0.5593 & -0.0522 & -0.0325 \\ 0.0483 & 0.0903 & 0.0195 & -0.0522 & 1.4071 & -0.0231 \\ 0.0587 & 0.0166 & -0.0343 & -0.0325 & -0.0231 & 2.8889 \end{bmatrix} \cdot 10^5$$

Fig. 17 Values of the mean stiffness matrix $\bar{K}$ obtained with the error ratios $\rho = 1.31$.

VII. Conclusions

The focus of this investigation was on the formulation and validation of a methodology for the estimation of an uncertain linear modal model of a structure from measurements of a few of its natural frequencies and mode shapes on a few nominally identical samples of the structure. The basis for the modal model is composed of the

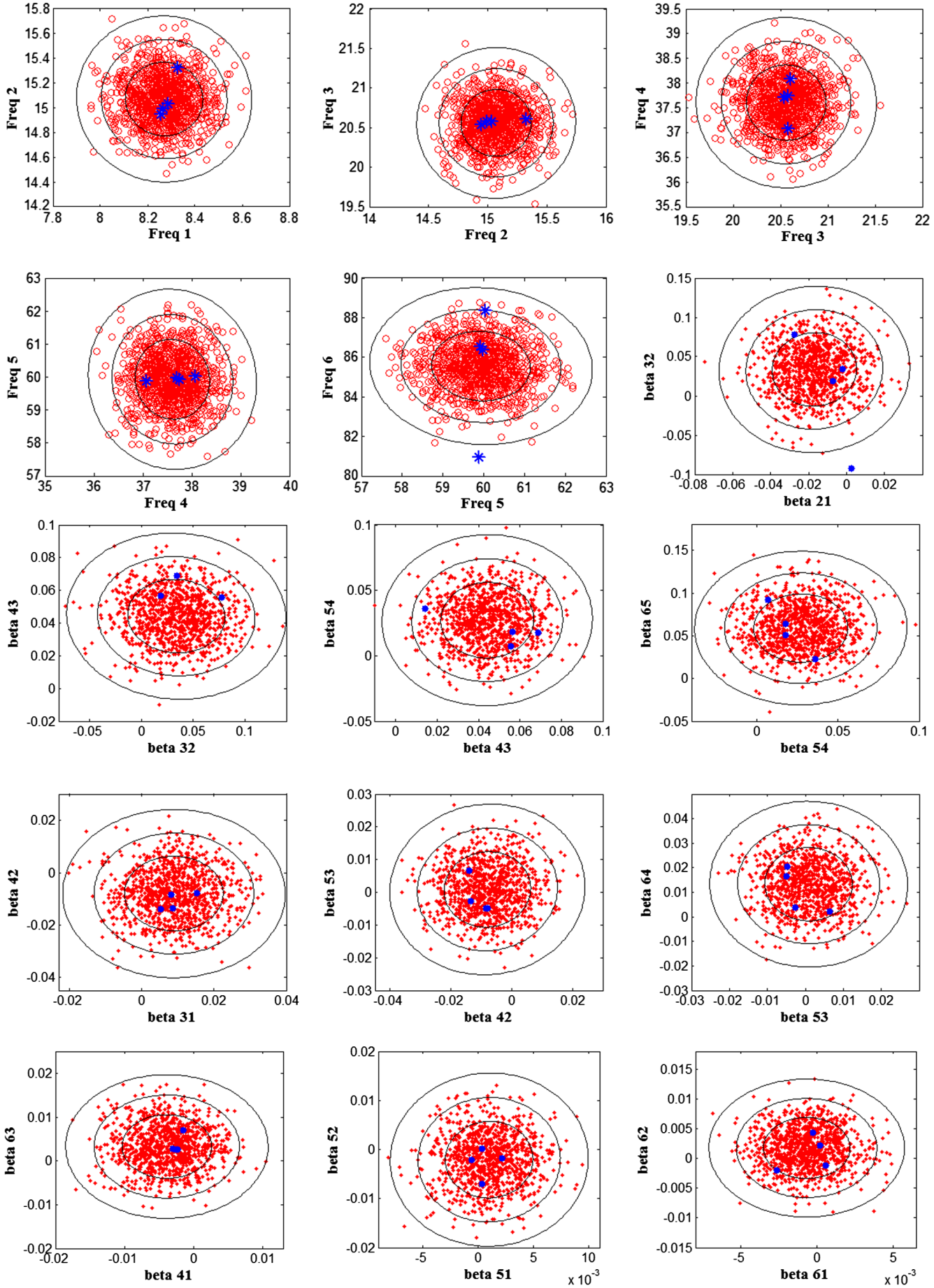

Fig. 18 Two-dimensional joint probability density functions of the natural frequencies (freq) and $\beta_{mj}^{(r)}$ values. Error ratio $\rho = 1.31$.

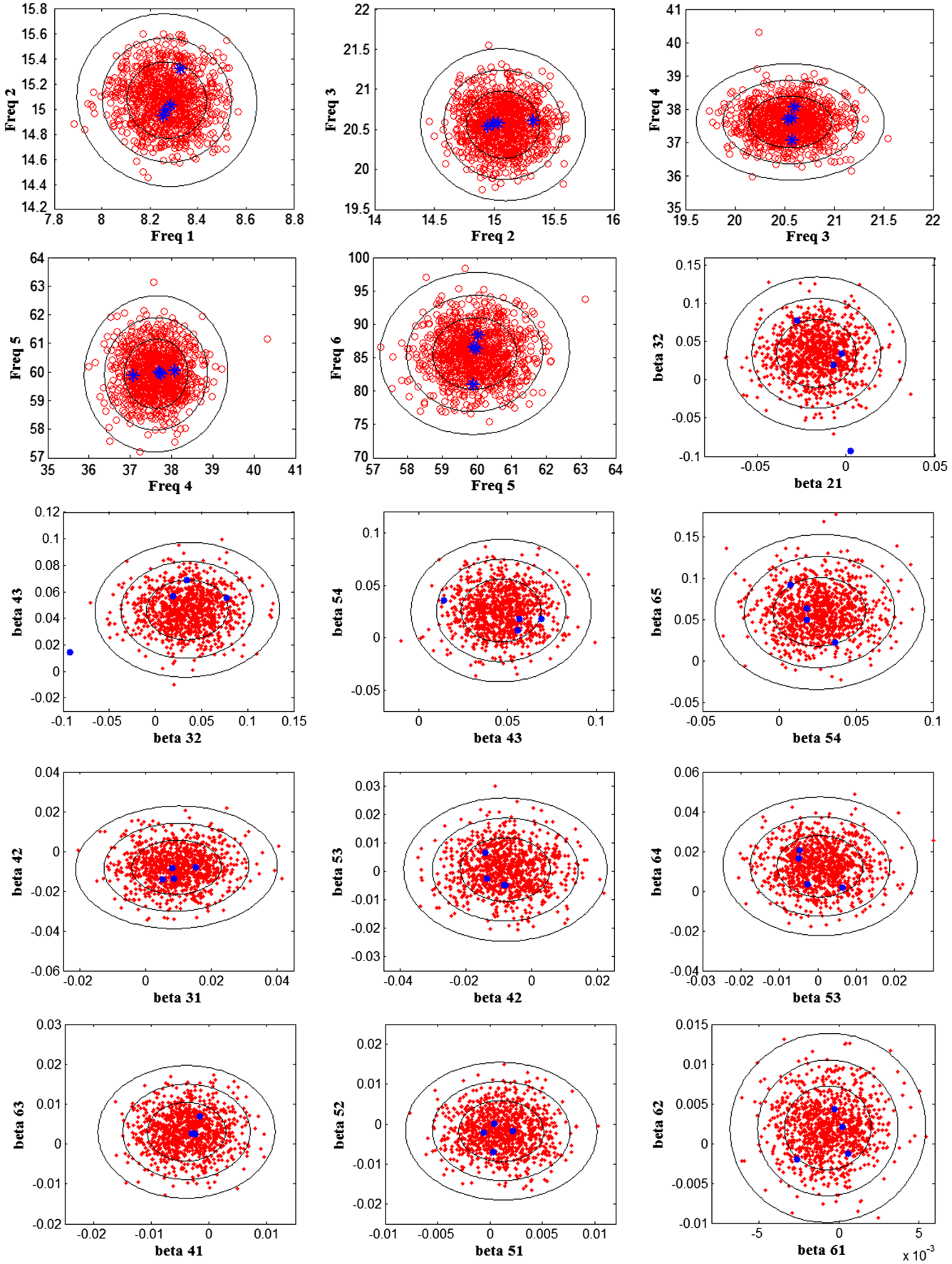

Fig. 19 Two-dimensional joint probability density functions of the natural frequencies (freq) and $\beta_{mj}^{(r)}$ values. Error ratio $\rho = 1.31$: nonparametric model of [4] for the last mode.

modes of an approximate representation of the structure, e.g., a nonupdated or preliminary FEM. The uncertainty in the structure was assumed to originate from stiffness properties with the stiffness matrix represented through the nonparametric stochastic modeling approach, i.e., Eqs. (1–3) and Fig. 1. To complete the modeling, it is thus necessary to estimate the mean stiffness matrix $\bar{K}$ and the parameter(s) of the nonparametric model, which was achieved using a maximum likelihood strategy. For computational expediency, the joint distribution of the natural frequencies and mode shape values necessary in this strategy was approximated by a joint Gaussian probability density function.

A critical step in this effort is the reduction of the mode shape data to information relevant to the modal model. In the tests considered here, M mode shapes of every sample of the structure would be measured at a large number n_L of locations that likely match a subset of nodes of the available FEM. However, the information needed for the estimation of the uncertain modal model parameters is the representation of these measured modes as linear combinations of the basis functions. This task was first accomplished through a least-squares projection [see Eq. (5)] of the measured modes on the basis. This data cannot be used directly for the estimation of the uncertain model parameters because of the lack of orthogonality of the measured modes with respect to the mass matrix, a property that is automatically satisfied by the uncertain modes of the model. The orthornormality of the modes was seen to represent constraints between the $M \times M$ projection coefficients so that only $M \times (M - 1)/2$ of those can in fact be considered independent. On this basis, it was proposed to reduce further the modal information to the skew-symmetric part of the projection coefficient matrix; see Eqs. (23–27).

The estimation of the uncertain model parameters from such data for the AFIT joined wing led, however, to an uncertainty level much larger than could be expected from the small variability of the natural frequencies. A detailed analysis of this issue demonstrated that it arises from the influence of noise on small projection coefficients. The noise effects were then lessened by modifying the least-squares projection of the measured modes on the basis: allowing a slightly larger error in the projection but constraining a better fit with the uncertain modal model structure; see Eqs. (29–32) and Fig. 13. The estimation of the uncertain modal model parameters, i.e., the mean stiffness matrix $\overline{K}$ and the parameter(s) of the nonparametric representation, was then achieved successfully; see Figs. 17–19. The methodology proposed here is applicable to a broad class of linear structures and data, e.g., accelerometer vs laser vibrometer, dense vs sparse measurements, etc.

Acknowledgment

The support of this research by the U.S. Air Force Research Laboratory Air Vehicles Summer Research Program to J. Avalos and M. P. Mignolet is gratefully acknowledged.

References

[1] Pitt, D., Haudrich, D., Thomas, M., and Griffin, K., "Probabilistic Aeroelastic Analysis and Its Implications on Flutter Margin Requirements," 49th Structures, Structural Dynamics, and Materials Conference, Schaumburg, IL, AIAA Paper 2008-2198,April 2008.

[2] Boston, J., Swenson, E., Kunz, D., Yu, W., and Blair, M., "Experiments with Geometric Non-Linear Coupling for Analytical Validation," 51st Structures, Structural Dynamics, and Materials Conference, Orlando, FL, AIAA Paper 2010-3018, April 2010.

[3] Soize, C., "A Nonparametric Model of Random Uncertainties in Reduced Matrix Model in Structural Dynamics," *Probabilistic Engineering Mechanics*, Vol. 15, 2000, pp. 277–294. doi:10.1016/S0266-8920(99)00028-4

[4] Mignolet, M. P., and Soize, C., "Nonparametric Stochastic Modeling Of Linear Systems With Prescribed Variance Of Several Natural Frequencies," *Probabilistic Engineering Mechanics*, Vol. 23, 2008, pp. 267–278. doi:10.1016/j.probengmech.2007.12.027

[5] Benjamin, J. R., and Cornell, C. A., *Probability, Statistics, and Decision for Civil Engineers*. McGraw–Hill, New York, 1970.

[6] Chen, C., Duhamel, D., and Soize, C., "Probabilistic Approach for Model and Data Uncertainties and its Experimental Identification in Structural Dynamics: Case of Composite Sandwich Panels," *Journal of Sound and Vibration*, Vol. 294, 2006, pp. 64–81. doi:10.1016/j.jsv.2005.10.013

[7] Soize, C., Capiez-Lernout, E., Durand, J. F., Fernandez, C., and Gagliardini, L., "Probabilistic Model Identification of Uncertainties in Computational Models For Dynamical Systems and Experimental Validation," *Computer Methods in Applied Mechanics and Engineering*, Vol. 198, 2008, pp. 150–163. doi:10.1016/j.cma.2008.04.007

[8] Durand, J. F., Soize, C., and Gagliardini, L., "Structural-Acoustic Modeling of Automotive Vehicles in Presence of Uncertainties and Experimental Identification and Validation," *Journal of the Acoustical Society of America*, Vol. 124, No. 3, 2008, pp. 1513–1525. doi:10.1121/1.2953316

[9] Batou, A., and Soize, C., "Identification of Stochastic Loads Applied to a Non-Linear Dynamical System Using an Uncertain Computational Model and Experimental Responses," *Computational Mechanics*, Vol. 43, No. 4, 2009, pp. 559–571. doi:10.1007/s00466-008-0330-y

[10] Kiflu, B., *Analysis of Mistuned Bladed Disks by a Reduced Order Technique: Validation, Identification, and Stochastic Modeling*, M.S. Thesis, Arizona State Univ., Phoenix, AZ, May 2005.

[11] Bowman, A. W., and Azzalini, A., *Applied Smoothing Techniques for Data Analysis*, Oxford Univ. Press, Oxford, England, U.K., 1997.

[12] Terrell, G. R., and Scott, D. W., "Variable Kernel Density Estimation," *Annals of Statistics*, Vol. 20, No. 3, 1992, pp. 1236–1265. doi:10.1214/aos/1176348768

[13] Soize, C., "A Computational Inverse Method for Identification of Non-Gaussian Random Fields Using the Bayesian Approach in Very High Dimension," *Computer Methods in Applied Mechanics and Engineering*, Vol. 200, No. 45–46, 2011, pp. 3083–3099. doi:10.1016/j.cma.2011.07.005

[14] Omar, E., "Sensor Integration Study for Sensor Craft UAV Mid-Term Review," Contract F33615-00-D-3052, Delivery Order: 0019, The Boeing Co., Presentation Material, Seattle, WA, Sept. 2003.

[15] Lee, H. A., Kim, Y. I., Park, G. J., Kolonay, R. M., Blair, M., and Canfield, R. A., "Structural Optimization of a Joined-Wing Using Equivalent Static Loads," *Journal of Aircraft*, Vol. 44, No. 4, 2007, pp. 1302–1308. doi:10.2514/1.26869

[16] Narayanan, V., "Structural Analysis of Reinforced Shell Wing Model For Joined-Wing Configuration," M.S. Thesis, Univ. of Cincinnati, Cincinnati, OH, 2005.

[17] Wolkovich, J., "The Joined-Wing: An Overview," *Journal of Aircraft*, Vol. 23, No. 3, 1986, pp. 161–178. doi:10.2514/3.45285

[18] Blair, M., and Striz, A. G., "Finite Element Beam Assemblies with Geometric Bend–Twist Coupling," 49th Structures, Structural Dynamics, and Materials Conference, Schaumburg, IL, AIAA Paper 2008-1796, April 2008.

[19] Patil, M. J., "Nonlinear Aeroelastic Analysis of Joined-Wing Aircraft," 44th Structures, Structural Dynamics, and Materials Conference, Norfolk, VA, AIAA Paper 2003-1487, April 2003.

[20] Snyder, R. D., Hur, J., Strong, D., and Beran, P., "Aeroelastic Analysis of a High-Altitude Long-Endurance Joined-Wing Aircraft," 46th Structures, Structural Dynamics, and Materials Conference, Austin, TX, AIAA Paper 2005-1948, April 2005.

[21] Blair, M., Canfield, R., and Roberts, R., "A Joined-Wing Aeroelastic Design with Geometric Non-Linearity," *Journal of Aircraft*, Vol. 42, No. 4, pp. 832–848, 2005. doi:10.2514/1.2199.

[22] Smallwood, B. P., "Structurally Integrated Antennas on a Joined-Wing Aircraft," M.S. Thesis, Air Force Inst. of Technology, Wright-Patterson AFB, OH, March 2003.

[23] Roberts, R., "Sensor-Craft Analytical Certification," M.S. Thesis, Air Force Inst. of Technology, Wright-Patterson AFB, OH, March 2003.

[24] Bond, V., and Canfield, R. A., "Wind Tunnel Testing of a Twisted Wing for Longitudinal Control in a Joined-Wing Aircraft," 48th Structures, Structural Dynamics, and Materials Conference, Honolulu, HI, AIAA Paper 2007-1772, April 2007.

[25] Niedbal, N., "Analytical Determination of Real Normal Modes from Measured Complex Responses," 25th Structures, Structural Dynamics and Materials Conference, Palm Springs, CA, AIAA Paper 1984-0995, 1984.